

# A neutron halo in ${}^8\text{He}$

A. V. Nesterov, V. S. Vasilevsky, O. F. Chernov  
Bogolyubov Institute for Theoretical Physics,  
Ukrainian Academy of Sciences, 252143, Kiev 143, Ukraine

October 31, 2018

## Abstract

The structure of  ${}^8\text{He}$  is investigated within a three-cluster microscopic model. The three-cluster configuration  $\alpha + {}^2n + {}^2n$  was used to describe the properties of the ground state of the nucleus. The obtained results evidently indicate the existence of a neutron halo in  ${}^8\text{He}$ .

## 1 Introduction

The development of the experimental technique made it possible to investigate light nuclei with large neutron excess, i.e., the nuclei for which the ratio  $\eta = (N - Z)/A$  is significantly larger than for common ones. Such nuclei lie near the drip line and are  $\beta$ -unstable. They live a short time and transform by emitting electrons into nuclei with approximately equal number of protons and neutrons. A number of unexpected properties were discovered in those nuclei, for instance, a neutron halo. It is natural that many attempts were undertaken to explain those properties within microscopic and semi-microscopic methods [1, 2, 3, 4, 5, 6, 7, 8].

Our aim is to investigate the structure of the  ${}^8\text{He}$  ground state. It is interesting that  ${}^8\text{He}$  has the largest value of  $\eta = 0.5$  among other nucleon-stable nuclei. Note that the average values of  $\eta = 0.4$  for nuclei near the neutron drip line. As early as in 1960, Ya. B. Zeldovich [9] and V. I. Goldansky [10] indicated a possibility of the existence of  ${}^8\text{He}$  isotope. It was experimentally confirmed [11] in the middle of sixties. The subsequent analysis shows that the lowest threshold of  ${}^8\text{He}$  decay is  ${}^6\text{He} + 2n$  and lies 2.1 MeV above the ground state and energy of the threshold  $\alpha + 4n$  equals 3.10 MeV (see, for instance, [12]).

The most complete information on light nuclei with neutron excess can be obtained with a microscopic model. In this case, the problem is connected with solving the many-particle Schrödinger equation with a fixed (chosen) nucleon-nucleon interaction. The equation has to be solved with some simplification based on one or other physical considerations. The Resonating Group Method [13] or its Algebraic Version [14, 15] is one of such methods.

In this paper, we make use of the Algebraic Version of the Resonating Group Method in which  ${}^8\text{He}$  is considered as a three-cluster configuration  $\alpha + {}^2n + {}^2n$ . It is obvious that

we make *a priori* some assumptions on the structure of the nucleus. First, wave functions of each cluster are modelled by the shell-model functions. Second, valent neutrons unite in dineutron clusters. As a justification for such an assumption can be served the fact, indicated by A. B. Migdal [16], that the interaction between two neutrons may be increased significantly in the presence of the third particle. It can give rise to the creation of the dineutron clusters on the surface of a nucleus. The chosen clusterization allow us to consider an  $\alpha$ -particle as a core, despite that the lowest threshold of  ${}^8\text{He}$  decay is  ${}^6\text{He}+n+n$ . Earlier, A. A. Ogloblin [17] indicated the importance of a cluster configuration  $\alpha + 4n$ . He pointed out that the bound energy of two neutrons in  ${}^8\text{He}$  is two times larger than that in  ${}^6\text{He}$ . This fact led him to the conclusion that  ${}^6\text{He}$  cannot serve as a core and the neutron halo in  ${}^8\text{He}$  has to be consisted of four neutrons.

Note also that the usage of dineutron clusters is a quite grounded approximation. For example, in [18], dineutron and also diproton clusters were successfully used to describe exit channels of the reactions  ${}^3\text{H}+{}^3\text{H}\rightarrow{}^4\text{He}+n+n$  and  ${}^3\text{He}+{}^3\text{He}\rightarrow{}^4\text{He}+p+p$  respectively. Besides, in [19], main features of  ${}^{11}\text{Li}$  was reproduced within the cluster configuration  ${}^9\text{Li}+{}^2n$  with a pointless dineutron.

## 2 Method

The present method for investigation of the  ${}^8\text{He}$  ground state is based on the Algebraic Version of the Resonating Group Method (AV RGM). For a long time, this version was used for studying the bound states of two-cluster systems, reactions with a few open channels, interaction of these channels with collective monopole and quadrupole modes, and also processes of full disintegration of light nuclei [20, 21, 22]. Recently, the AV RGM was actively applied to describe three-cluster systems [23, 24, 25, 26].

The Algebraic Version of the Resonating Group Method is based on the usage of an oscillator basis for solving bound state problems and problems of continuous spectrum states. This is achieved by expanding a wave function of inter-cluster motion in the oscillator basis. As a result, a trial three-cluster function takes the form

$$\Psi(A) = \sum_n C_n \hat{A} [\Phi_1(A_1)\Phi_2(A_2)\Phi_3(A_3)f_n(\mathbf{q}_1, \mathbf{q}_2)], \quad (1)$$

where  $\hat{A}$  is the antisymmetrization operator,  $\Phi_i(A_i)$  are the internal functions of the cluster, which are selected in one or other form prior to solving the problem (for instance, in the form of many-particle oscillator shell functions as in our case); the set of coefficients  $C_n$  is nothing else but a wave function in the oscillator representation. This function should be obtained from a system of linear equations:

$$\sum_{n'} \left[ \langle n, | \hat{H} | n' \rangle - E \langle n | n' \rangle \right] C_{n'} = 0, \quad (2)$$

which is derived directly from the many-particle Schrödinger equation. The oscillator functions  $f_n(\mathbf{q}_1, \mathbf{q}_2)$ , where  $\mathbf{q}_1$  and  $\mathbf{q}_2$  are Jacobi vectors fixing a position of clusters in space, are determinate in the six-dimensional space and constitute the irreducible representation  $[N00]$  of the unitary group  $U(6)$ . Thus, the composite index  $n$  consists of indices (six in total) of the irreducible representation of the  $U(6)$  group and its subgroups.

The choice of one or other reductions of the  $U(6)$  group is dictated by considerations of physical lucidity and simplicity of numerical realizations as well. To consider the bound state problem, it is convenient to use bases, whose classification is connected with the following reduction of the  $U(6)$  group:

$$\begin{aligned}
U(6) \supset \begin{array}{c} U(3) \otimes U(3) \\ \cup \qquad \cup \\ SO(3) \otimes SO(3) \supset SO(3) \end{array} & \implies |N_1 l_1, N_2, l_2, LM \rangle \\
U(6) \supset \begin{array}{c} SU(3) \otimes U(2) \\ \cup \qquad \cup \\ SO(3) \quad O(3) \end{array} & \implies |(\lambda\mu)\nu, \omega LM \rangle
\end{aligned}$$

The first basis is usually called the basis of two uncoupled oscillators or bioscillator basis (BO). Each of the  $SU(3)$  groups, associated with one of the Jacobi vectors  $\mathbf{q}_1$  and  $\mathbf{q}_2$ , generates the quantum numbers  $N_1, l_1$  and  $N_2, l_2$ . They are the principal quantum number (or the number of oscillator quanta) and partial angular momentum along the respective Jacobi vector:

$$|N_1, l_1, N_2, l_2; LM \rangle$$

The second basis is an " $SU(3)$ " basis. Wave functions of this basis are classified through the well-known Elliott indices  $(\lambda, \mu)$  of the  $SU(3)$  group, multiplicity index  $\omega$  arising in the reduction  $SU(3) \subset SO(3)$ , and quantum number  $\nu = \frac{1}{2}(N_1 - N_2)$  connected with oscillator quanta along the Jacobi vectors  $\vec{q}_1$  and  $\vec{q}_2$ :

$$|(\lambda\mu)\nu; \omega LM \rangle$$

The total number of oscillator quanta equals  $N = N_1 + N_2 = \lambda + 2\mu$  and defines the irreducible representation of the  $U(6)$  group. For a given  $N$ , i.e., for a fixed oscillator shell, functions of both bases related to each other through a unitary transformation, because these bases are eigenfunctions of the same oscillator hamiltonian in the six-dimensional space. Thus, they are equivalent. Note that the unitary matrix connecting these two bases consists of the Clebsch-Gordan coefficients of the  $SU(3)$  group for the decomposition of the product  $(N_1 0) \otimes (N_2 0) \Rightarrow (\lambda\mu)$ . Thus

$$|(\lambda\mu)\nu; \omega LM \rangle = \sum_{l_1, l_2} U(N_1, l_1, N_2, l_2; (\lambda\mu)\nu; \omega) |N_1, l_1, N_2, l_2; LM \rangle$$

However we make use of two bases. This is because the bioscillator basis has more natural quantum numbers. Meanwhile, the  $SU(3)$  basis is more convenient for numerical implementation, in particular, for eliminating Pauli-forbidden states. Besides, the usage of two bases gives additional information on optimal subspaces, which allow one to obtain reliable results with minimal effort.

The elimination of Pauli-forbidden states is performed by diagonalization of the matrix of the antisymmetrization operator

$$\| \langle n | n' \rangle \|, \tag{3}$$

calculated between the basis functions (1). Pauli-forbidden states correspond to those eigenfunctions of the matrix  $\| \langle n | n' \rangle \| = \| \langle n | \hat{A} | n' \rangle \|$  which have zero eigenvalues.

Pauli-allowed states are a combination of original basis functions of a given oscillator shell which are eigenfunctions of the antisymmetrization operator. It should be noted that the matrix  $\| \langle n | n' \rangle \|$  has a block structure. Non-zero matrix elements correspond to overlapping basis functions of the same oscillator shell, i.e. those oscillator functions which obey the condition  $N = N'$ . To solve the Schrödinger equation in matrix form, one has to eliminate Pauli-forbidden states. Let us  $e_\alpha$  and  $\{U_n^\alpha\}$  be respectively eigenvalue and eigenfunction of the antisymmetrization operator. Then, the system of equations (2) should be transformed to the representation of Pauli-allowed states:

$$\sum_{\alpha'} \left[ \langle \alpha | \hat{H} | \alpha' \rangle - E \delta_{\alpha, \alpha'} \right] C_{\alpha'} = 0, \quad (4)$$

where  $\| \langle \alpha | \hat{H} | \alpha' \rangle \|$  is a matrix of hamiltonian between Pauli-allowed states connected with the matrix  $\| \langle n | \hat{H} | n' \rangle \|$  by the relation

$$\langle \alpha | \hat{H} | \alpha' \rangle = \sum_{n, n'} U_n^\alpha \langle n | \hat{H} | n' \rangle U_{n'}^{\alpha'}$$

In this connection, for the bioscillator basis the original scheme of classification is totally changed, but the quantum numbers  $(\lambda\mu)$  are preserved for the  $SU(3)$  basis, because the matrix  $\| \langle n | n' \rangle \|$  is off-diagonal with respect to the quantum number  $\nu$  only.

We omit all details of matrix elements calculations of the microscopic hamiltonian and antisymmetrization operator, by referring reader to the paper [27] where one can find basic formulae and recurrence relations for matrix elements of operators of the physical importance between bioscillator functions.

### 3 Results

Results, represented in this chapter, were obtained with the Volkov potential [28]. The only free parameter, oscillator radius  $r_0$ , was chosen to minimize the threshold energy of the  ${}^8\text{He}$  decay into  ${}^4\text{He}$  and two dineutrons. It turns out to be 1.51 fm. Under such conditions, the energy of the  ${}^4\text{He} + {}^2n + {}^2n$  threshold equals -22.15 MeV and the bound state energy of  $\alpha$ -particle is -26.84 MeV. Coulomb interaction was neglected because it leads to a shift of the bound state energy and threshold energy by the same value.

In what follows, we use two different trees of Jacobi vectors. In the first tree which we call "T"-tree, the vector  $\mathbf{q}_1$  defines the distance between two dineutrons, and the vector  $\mathbf{q}_2$  fixes the distance between the center of mass of two dineutrons and  $\alpha$ -particle. The second tree is called Y-tree. In this tree, the first vector  $\mathbf{q}_1$  determines the distance between  $\alpha$ -particle and one of the dineutrons, and the second vector  $\mathbf{q}_2$  is connected with the distance between the second dineutron and center of mass of the first dineutron and  $\alpha$ -particle.

As we concern with the ground state only, then we need to use wave function of the S-state. In this case oscillator basis is reduced significantly. For instance, the bioscillator basis involves oscillator functions with even values of  $N_1$  and  $N_2$ . Besides, partial angular momentum  $l_1 = l_2$ . Actually, we need only three quantum numbers to classify basis

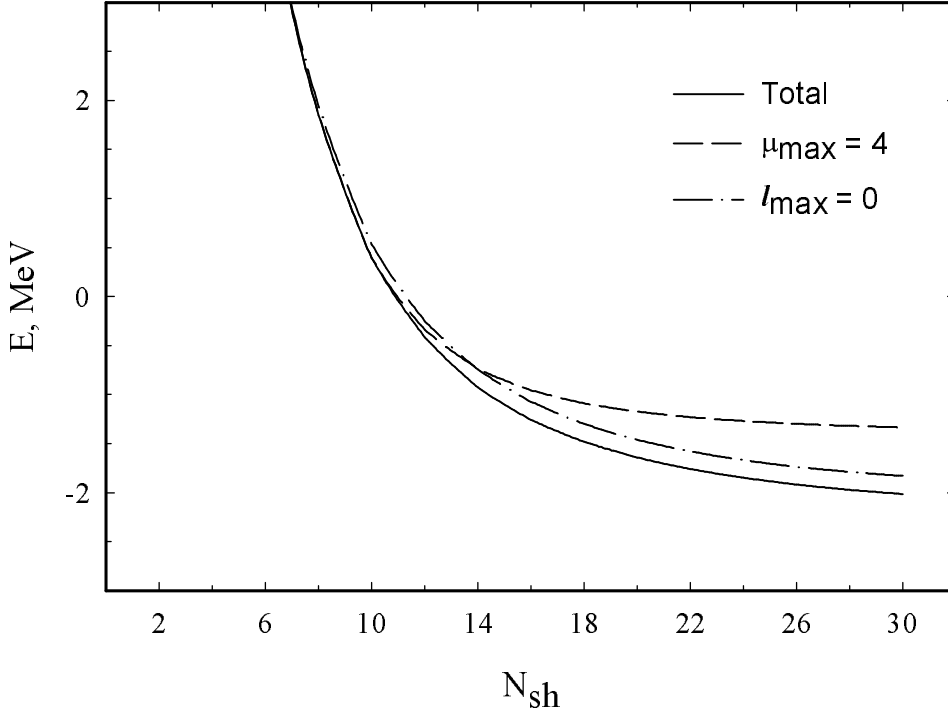


Figure 1:  ${}^8\text{He}$  ground state energy as a function of the number  $N$  of oscillator shells involved in the calculation.

functions with  $L = 0$ . They are  $(N_1, N_2, l = l_1 = l_2)$  for bioscillator basis, and  $(\lambda\mu, \nu)$  for  $SU(3)$  basis.

**Bound state energy and optimal subspaces.** The ground state of  ${}^8\text{He}$  is considered with the basis which involves all oscillator functions of 15 lowest oscillator shells, i.e., basis functions with even values of the principal quantum number  $N$  up to  $N = 30$ . The total number of the original basis functions equals 815 and the total number of Pauli-allowed states reduces to 399 functions. Such a number of basis functions provides a fairly good convergence of the bound state energy, as is demonstrated in Fig. 1. In this figure, we display the ground state energy as a function of the principal quantum number  $N$ . The energy is counted from the threshold  $\alpha + {}^2n + {}^2n$ . In Fig. 1, we also display the ground state energy obtained with some subspaces of the total space of the oscillator basis used. In the BO basis, such a subspace is defined by the maximal value of the partial angular momentum  $l = 0$ , while, for  $SU(3)$ -basis, such a subspace involves basis functions with  $\mu \leq 4$ . The later subspace consisting of 274 functions gives the energy which noticeable differs from "exact" one, obtained with the total basis. But, with the former subspace including only 118 functions, we obtain the energy which is very close to the "exact" value. This is probably connected with that the interaction between clusters is most strong in the  $S$ -state.

In Fig. 2, we display the wave function of the  ${}^8\text{He}$  ground state, more exactly, the coefficients  $C_\alpha$  of expansion over Pauli-allowed states. Two labels  $N_{sh}$  and  $N_{a.s.}$  are used to classify Pauli-allowed functions ( $\alpha = \{N_{sh}, N_{a.s.}\}$ ). The first label  $N_{sh}$  numerates oscillator shells and the second one,  $N_{a.s.}$ , numerates Pauli-allowed states of a given oscillator shell.

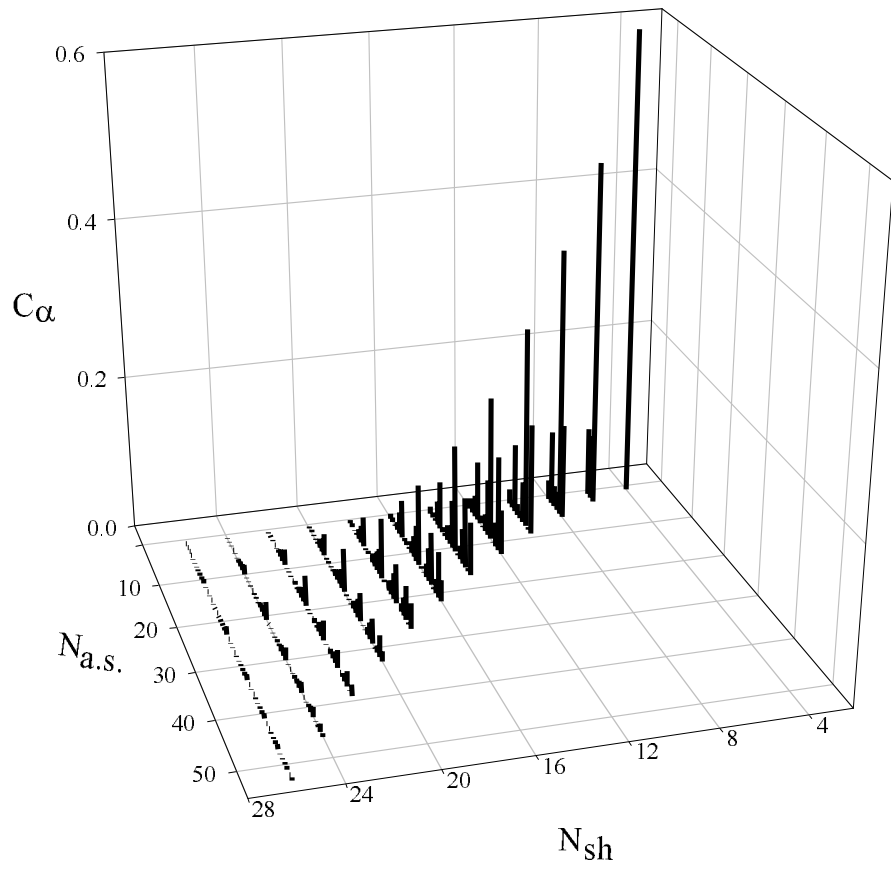


Figure 2: Wave function of the  $^8\text{He}$  ground state in oscillator representation.

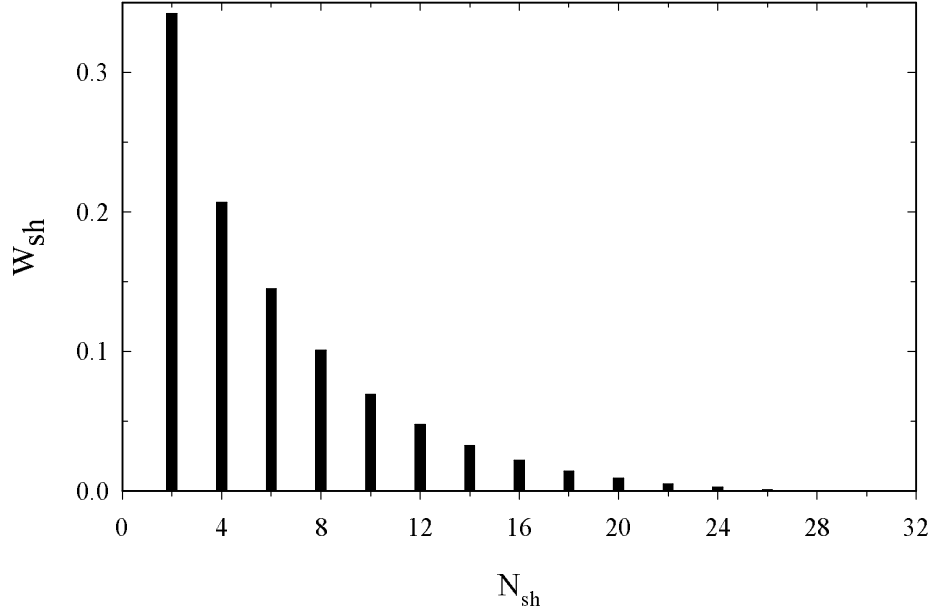


Figure 3: Contribution of different oscillator shells  $N$  to the wave function of the  ${}^8\text{He}$  ground state.

The expansion coefficients  $C_\alpha$  were determined in the  $SU(3)$ -basis, where the indices  $(\lambda\mu)$  are good quantum numbers after eliminating Pauli-forbidden states. The detailed analysis shows that the main contribution (around 80%) to the wave function comes from the basis states with  $\mu = 2$ , while the basis states with  $\mu = 0$  give only 9%. Note that the former states in  ${}^6\text{He}$  (see [23], [24]) were a dominated subspace with the contribution of more than 93%.

It is seen from Fig.2 and more clearly from Fig. 3 (where weights of different oscillator shells are displayed) that the main contribution comes from the lowest oscillator shells, however the contribution of shells with large  $N$  is also noticeable. It indicates a substantial clusterization of the nuclei, i.e., for a large amount of time, valent neutrons move far from the  $\alpha$ -particle, making a neutron halo.

In order to obtain additional information on the role of different subspaces of the total space of oscillator functions, we impose various restrictions on the quantum numbers of basis states. First, for the bioscillator basis we took a subspace with the maximal value of partial angular momenta ( $l = l_1 = l_2$ )  $l = 0$ ,  $l = 2$  and  $l = 4$ . It was made for both  $Y$ - and  $T$ -trees of Jacobi vectors. For the  $SU(3)$ -basis, we used only  $T$ -tree and the restriction was imposed on the maximal value of  $\mu = 0$ , 2 and 4. Results of such calculations are presented in Table 1. One can see that subspace  $l_1 = l_2 \leq 2$  for  $Y$ -tree of the bioscillator basis is the most optimal part of the total basis, because 54% of the total basis (or 219 functions) gives the ground state energy very close to the "exact" value.

**Effects of the Pauli principle.** To understand the role of the Pauli principle in a three-cluster system, we investigate the contribution of different Pauli-allowed states to the wave function of ground state. Each of Pauli-allowed states, being an eigenfunction of the

Table 1: Ground state energy of  ${}^8\text{He}$  counted from the threshold  ${}^4\text{He} + {}^2n + {}^2n$ .

Basis	Jacobi tree	Subspace	E, MeV	Number of functions
BO	T	Total	-2.065	399
		$l = 0$	-1.832	118
		$l \leq 2$	-2.047	219
		$l \leq 4$	-2.064	293
BO	Y	Total	-2.065	399
		$l = 0$	-1.839	118
		$l \leq 2$	-2.065	219
SU(3)	T	Total	-2.065	399
		$\mu = 0$	6.341	91
		$\mu \leq 2$	0.172	196
		$\mu \leq 4$	-1.335	274

antisymmetrization operator, can be marked (characterized) by corresponding eigenvalue of this operator. As we mentioned above, the antisymmetrization operator overlaps only those functions which obey the relation  $N_1 + N_2 = N'_1 + N'_2$ , i.e., basis functions of the same oscillator shell. Analysis of the eigenfunctions shows, that the diagonalization of the matrix  $\| \langle n | \hat{A} | n' \rangle \|$  reveals states with definite eigenvalues of the antisymmetrization operator for a two-cluster subsystem. This means, in particular, that the Pauli-forbidden state of three-cluster system is a state when at least one pair of clusters is in Pauli-forbidden state. For example, for the two-cluster subsystem  $\alpha + {}^2n$ , the oscillator functions with the number of oscillator quanta (along the inter-cluster coordinate)  $N = 0$  and  $N = 1$  are Pauli-forbidden states. In the subsystem  ${}^2n + {}^2n$ , where symmetry of the subsystem allows only even functions, we have only one forbidden state with  $N = 0$ . As for Pauli-allowed states for three-cluster system, they describe the states of the system, when all pairs of two-cluster subsystems are out of the Pauli-forbidden region.

To prove these statements, we consider eigenvalues of the antisymmetrization operator (which we denote by  $\lambda_\alpha$ ) for Pauli-allowed states and expansion coefficients  $C_\alpha$  over these states for oscillator shell  $N_{sh} = 20$ . These quantities, obtained in the  $SU(3)$  basis, are displayed in Fig. 4. Seven first functions correspond to the  $SU(3)$  irreducible representation  $(\lambda\mu) = (20, 0)$ , next eight functions belong to the  $SU(3)$  irreducible representation  $(\lambda\mu) = (16, 2)$  and so on. Last function has the  $SU(3)$  symmetry  $(\lambda\mu) = (0, 10)$ . In this Figure by dashed horizontal lines we indicate the eigenvalues of the antisymmetrization operator for two-cluster subsystem  $\alpha + {}^2n$ . Note that corresponding values for the subsystem  ${}^2n + {}^2n$  equal 1. One can see indeed, that some eigenvalues of the operator  $\hat{A}$  for three-cluster system coincide with the eigenvalues of this operator for the subsystem  $\alpha + {}^2n$ . Besides, one notices that such states, corresponding to the even oscillator quanta  $N = 2$  and  $N = 4$  in the  $\alpha + {}^2n$  subsystem, play dominant role in the ground state of  ${}^8\text{He}$ .

**RMS radii.** In Table 2, we compare the calculated mass, neutron and proton root-mean-square (RMS) radii with available experimental data. The theoretical values of



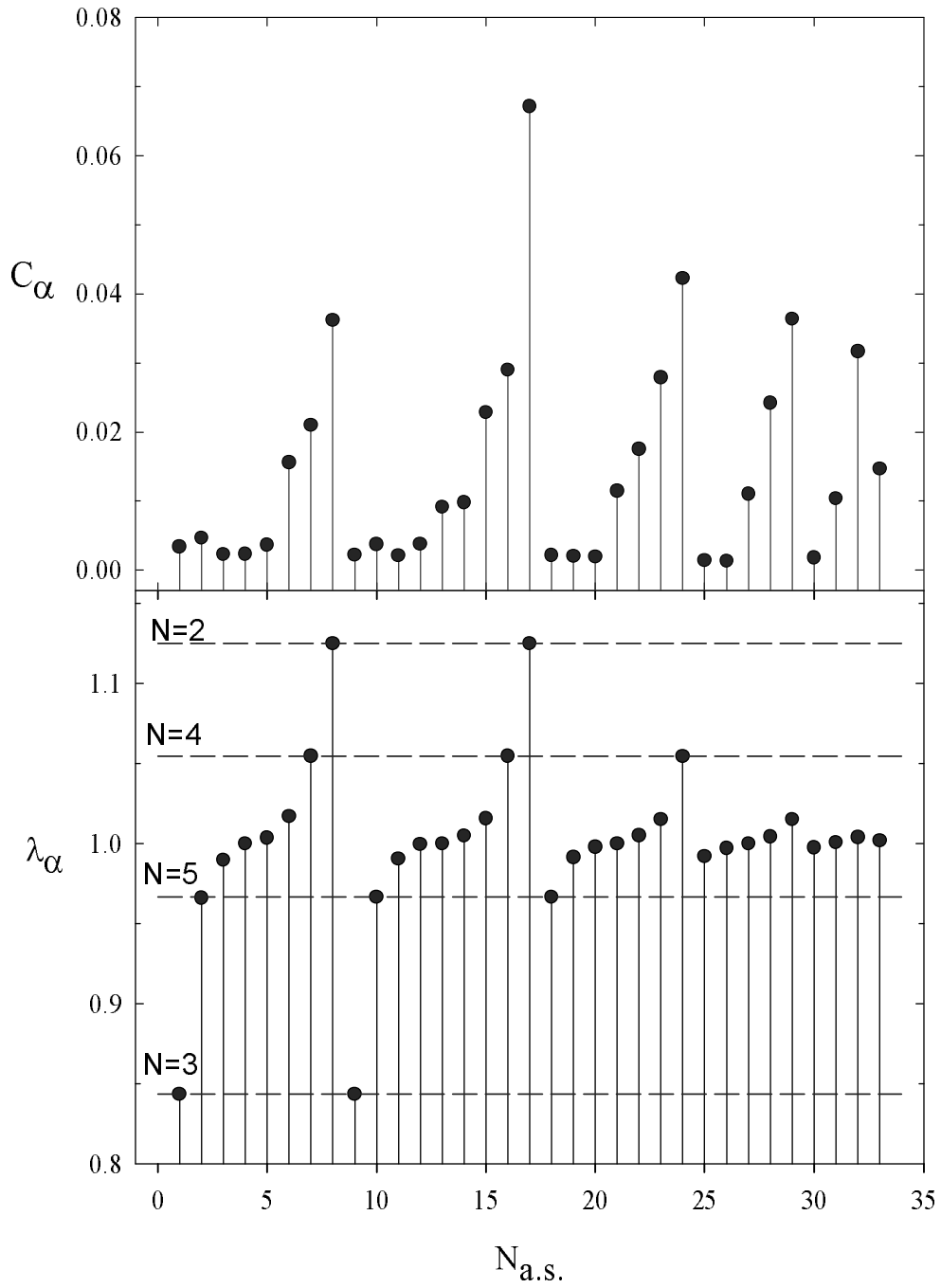


Figure 4: Eigenvalues of the antisymmetrization operator  $\lambda_{N_{a.s.}}$  and expansion coefficients  $C_\alpha$  for the oscillator shell  $N = 20$ .

Table 2: Root mean square radii for the ground state of  ${}^8\text{He}$ .

RMS, fm	Theory	Experiment [29]	Experiment [30]
RMSm	2.73	$2.37 \pm 0.18$	$2.52 \pm 0.03$
RMSp	2.08	$1.89 \pm 0.17$	$2.15 \pm 0.02$
RMSn	2.91	$2.50 \pm 0.19$	$2.64 \pm 0.03$
RMSn-RMSp	0.84	0.61	0.49

Table 3: Root mean square radii of  ${}^8\text{He}$ , obtained by different methods.

RMS, fm	AV RGM	RRGM [1]	Shell Model [4]
RMSm	2.73	2.41	
RMSp	2.08	1.71	1.684
RMSn	2.91		

RMS radii are a little larger than experimental ones which we took from [29] and [30].

This is perhaps because the calculated binding energy is a little less than the experimental one. But the present model correctly reproduces the general picture of  ${}^8\text{He}$ . One sees that radius of neutron matter is larger than the one of proton matter. The difference of these radii is 0.84 fm. These results also indicate the existence of a neutron halo in the nucleus.

In Table 3, we collected the mass, neutron and proton RMS radii, obtained with different theoretical methods: AV RGM (present calculations), the Refined Resonating Group Method (RRGM)[1], and Multi-configuration Shell Model [4].

**Shape of three-cluster system.** Having calculated the coefficients  $C_n$ , a wave function in the oscillator representation, we thus obtain the wave function for relative motion of the three-cluster system:

$$\Phi(\mathbf{q}_1, \mathbf{q}_2) = \sum_n C_n \phi_n(\mathbf{q}_1, \mathbf{q}_2). \quad (5)$$

By using (5), we can evaluate mean distance between clusters. For this aim, one has to calculate the following quantities:

$$\begin{aligned} Q_1^2 &= \int d\mathbf{q}_1 d\mathbf{q}_2 \Phi^*(\mathbf{q}_1, \mathbf{q}_2) \mathbf{q}_1^2 \Phi(\mathbf{q}_1, \mathbf{q}_2), \\ Q_2^2 &= \int d\mathbf{q}_1 d\mathbf{q}_2 \Phi^*(\mathbf{q}_1, \mathbf{q}_2) \mathbf{q}_2^2 \Phi(\mathbf{q}_1, \mathbf{q}_2), \end{aligned}$$

which, within the regard for the normalization of the wave function and definition of Jacobi coordinates, define the sought parameters. For instance, for  $T$ -tree, the mean value of  $q_1$  is connected with the base of an isosceles triangle and the mean value of  $q_2$  is connected with its height.

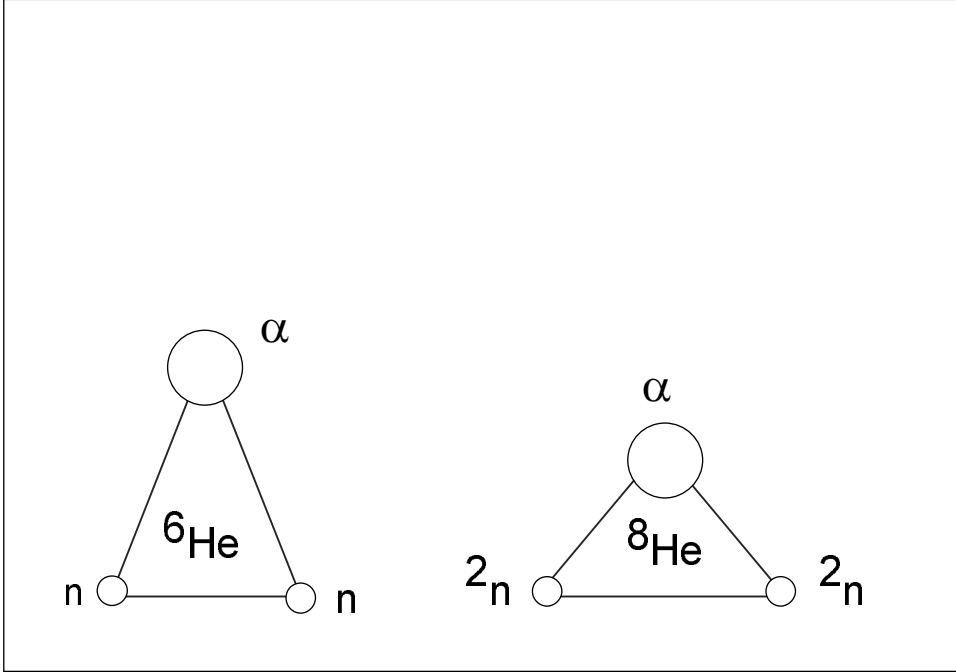


Figure 5: Shape of the triangles which are composed by three clusters in  ${}^8\text{He}$  and  ${}^6\text{He}$ .

The mean distance between two dineutrons turns out to be 2.33 fm and the mean distance between  $\alpha$ -particle and the center of mass of two dineutrons is 1.42 fm. Thus, in  ${}^8\text{He}$ , three clusters form an isosceles, almost rectangular triangle with  $\alpha$ -particle at the vertex of the right angle.

Note, that the situation is somewhat different for  ${}^6\text{He}$ . Clusters form an acute-angled triangle. Two valent neutrons in the presence of  $\alpha$ -particle make a subsystem with the RMS radius equal to 2.52 fm which is less than the RMS radius of a free deuteron (2.69 fm) calculated with the same potential and the same number of basis functions. These triangles are displayed in Fig. 5.

The difference in the geometry of cluster's disposition in  ${}^6\text{He}$  and  ${}^8\text{He}$  is more likely connected with the Pauli principle. There is an effective repulsion between two dineutrons, arising from the Pauli principle, which strives to place dineutrons on different sides the  $\alpha$ -particle. Contrary to the case of  ${}^8\text{He}$ , valent neutrons with opposite orientations of spins may unite in a rather compact subsystem in  ${}^6\text{He}$  (due to the presence of  $\alpha$ -particle).

**Density distribution.** Proton, neutron and mass density distributions also confirm the existence of a neutron halo in  ${}^8\text{He}$ . As seen from Fig. 6, where we display the proton, neutron and mass

density distributions for both  ${}^8\text{He}$  and  ${}^6\text{He}$ , the size of a neutron cloud is substantially larger than the size of a proton cloud. Besides, main part of neutrons in  ${}^8\text{He}$  move on the surface of the nucleus. One sees the depression in the neutron density distribution at small values of the coordinate  $r$ . This is due to the Pauli principle, which makes four neutrons (united in two dineutrons) move at a relatively large distance from the  $\alpha$ -particle.

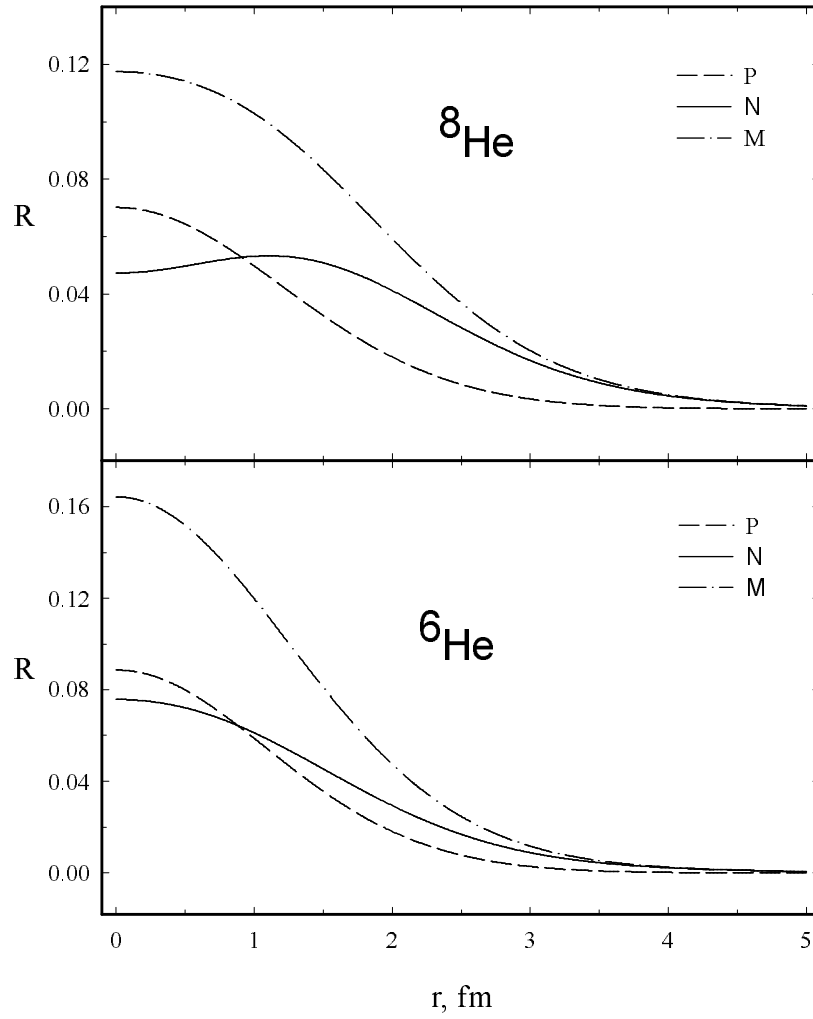


Figure 6: Proton, neutron and mass density distributions in  $^8\text{He}$  and  $^6\text{He}$ .

## 4 Conclusion

In this paper, we have investigated the ground state properties of  ${}^8\text{He}$  within the three-cluster microscopic model. The three-cluster configuration  ${}^4\text{He}+{}^2n+{}^2n$  was used to simulate the dynamics of the eight-nucleon system. The model suggested describes reasonably well parameters of the ground state: binding energy, mass, proton and neutron root-mean-square radii. The analysis of the system shows, that valent neutrons move at a large distance from  $\alpha$ -particle, forming a neutron halo in  ${}^8\text{He}$ .

## References

- [1] Wurzer. J. and Hofmann H. M. // Phys. Rev. 1997. **C55**. P.688.
- [2] Suzuki Y., Varga K. and Lovas R. G. // Nucl. Phys. 1994. **A571**. P.447.
- [3] Amos K., Karataglidis S., Dortmans P. J. and Bennhold C.// E-preprint. 1998. **nucl-th/9811045**.
- [4] Navratil P. and Barrett B. R.// E-preprint. 1998. **nucl-th/9804014**.
- [5] Zhukov M. V. et al.// Phys. Rep. 1993. **231**. P.151.
- [6] Danilin B. V. et al.// Phys. Rev. 1991. **C43**. P.2835.
- [7] Csoto A.// Phys. Rev. 1993. **C48**. P.165.
- [8] Ohbayasi Y., Varga K., Suzuki Y.// Phys. Rev. 1994. **C50**. P.189.
- [9] Zeldovich Ya. B.// Sov. J. Exp. Theor. Phys. 1960. **38**. P.1123.
- [10] Goldansky V. I.// Sov. J. Exp. Theor. Phys. 1960. **38**. P.1637.
- [11] Cerny J. et al.// Phys. Rev. Lett. 1966. **16**. P.469.
- [12] Ajzenberg-Selove F.// Nucl. Phys. 1988. **A490**. P.1.
- [13] Tang Y. and Wildermuth K.// A unified theory of the nucleus. Braunschweig: Vieweg Verlag, 1977.
- [14] Filippov G. F. and Okhrimenko I. P.// Sov. J. Nucl. Phys. 1981. **32**. P.480.
- [15] Filippov G. F.// Sov. J. Nucl. Phys. 1981. **33**. P.488.
- [16] Migdal A .B.// Yad. Fiz. 1972. **16**. P.427.
- [17] Ogloblin A. A.// Present status of exotic lightest nuclei. Proceedings of International Conference on Exotic Nuclei, Foros, Crimea, October, 1991, Edited by Yu. E. Penionzhkevich and R. Kalpakchieva, World Scientific, Singapore-New Jersey-London-Hong Kong. 1991. P.36.
- [18] Vasilevsky V. S. and Rybkin I. Yu.// Sov. J. Nucl. Phys. 1989. **50**. P.411.
- [19] Jonson B. and Hansen P. G.// Europhys. Lett. 1987. **4**. P.409.
- [20] Filippov G. F. et al.// Sov. J. Nucl. Phys. 1985. **43**. P.536.

- [21] Filippov G. F., Vasilevsky V. S. and Nesterov A. V.// Nucl. Phys. 1984. **A426**. P.327.
- [22] Filippov G. F., Vasilevsky V. S. and Nesterov A. V.// Sov. J. Nucl. Phys. 1984. **40**. P.901.
- [23] Vasilevsky V. S., Nesterov A. V., Arickx F., and Van Leuven P.// Preprint ITP-96-3E. 1996.
- [24] Vasilevsky V. S., Nesterov A. V., Arickx F., and Van Leuven P.// Physics of Atomic Nuclei (Yad. Fiz.). 1997. **60**. P.413.
- [25] Filippov G. F.// Yad. Fiz. 1999. **62**. P.1763.
- [26] Korennov S. V., Filippov G. F., Rybkin I. Yu. and Kato K.// J. Math. Phys. 1995. **36**. P.4571.
- [27] Nesterov A. V.// Yad. Fiz. 1993. **56**. P.35.
- [28] Volkov A. B.// Nucl. Phys. 1965. **74**. P.33.
- [29] Neumaier S. R., Alkhazov G. D., Andronenko G. D.// Scientific Report 1995, GSI 96-1, Roether Druk, Darmstadt. 1996.
- [30] Tanihata I. et al.// Phys. Lett. 1988. **B206**. P.592.